JOURNAL OF PROPULSION AND POWER
Vol. 13, No. 1, January–February 1997

Mass-Flux-Based Implicit Multigrid Method for Modeling Multidimensional Combustion

Xiaoqing Zheng,* Changming Liao,* Zhining Liu,† and Chaoqun Liu‡
University of Colorado, Denver, Colorado 80217

A highly accurate and efficient method for modeling three-dimensional reacting flows with detailed chemistry is described in this paper. A mass-flux-based governing system is developed for general curvilinear coordinates to obtain compactness of the discretization stencil. The momentum equations are represented by a set of equations of mass fluxes across cell interfaces, which are discretized by using staggered grid techniques. A third-order monotone upwind-biased scheme is used for all of the convection terms in the flow equations and species equations to minimize numerical diffusion and capture the sharp gradients existing in flames. The governing equations are divided into a chemical reaction part and a fluid flow part, and they are solved in a semicoupled way. An implicit semicoarsening multigrid method combined with a line-distributive relaxation is used as the flow solver. The species equations are discretized by an implicit method and solved in a fully coupled way. Computational results for a confined coflowing diffusion flame show good agreement with experimental data. A detailed three-dimensional calculation of combustion in a gas-turbine combustor with strong swirling inflows is also presented.

I. Introduction

TYPICAL combustion problems involve flow variables, temperature, and a large number of chemical species, and require the solution of the coupled equations of mass, momentum, species balance, and energy with detailed thermodynamic and transport relations and finite rate chemistry. Because of the strong interaction between fluid flow and chemical reaction, and severe stiffness and nonlinearity of chemical reaction terms, the governing equations are extremely difficult to solve. Furthermore, the large number of chemical species that must be solved at each grid point for detailed chemistry makes the computational cost extremely high.

In the past, numerical studies have followed two paths: 1) simple flow with detailed chemistry[1–6] or 2) complex flow with reduced chemistry.[7–11] For many years, detailed combustion simulation has been limited to simplified one- or two-dimensional test cases. With the rapid development of efficient numerical methods and powerful computers in recent years, simulation of combustion is now advancing to attack more practical problems, such as three-dimensional combustion with detailed chemistry.

This paper describes a very accurate and efficient numerical method developed for calculating general three-dimensional reacting flows with detailed chemistry. The principal focus is on the development of a highly efficient and accurate method for chemical species transport equations. Based on the finite volume frame, an implicit method is developed to solve the three-dimensional Navier–Stokes equations and chemical species transport equations in general curvilinear coordinates. A distinctive feature of this method is that the mass fluxes are employed as the dependent variables. The momentum equations of mass fluxes are discretized in staggered control volumes by using the techniques developed by Patankar,[12] whereas the energy equations and species equations are integrated basically by using a cell-centered finite volume scheme. In this way, the discretized mass equation remains as simple as in the Cartesian grids and the stencil is spatially the most compact. A third-order monotone upwind-biased scheme[13,14] is used for all of the convection terms of flow equations and species equations to minimize numerical diffusion and maintain the sharp gradients existing in flames.

This method was tested by calculating a confined coflowing methane–air diffusion flame and strong swirling combustion in a three-dimensional gas-turbine combustor. Comparison with experimental data is made for the first case.

II. Governing Equations

The governing equations for general compressible reacting flows in integration form can be summarized as follows.

Mass conservation:

$$\int_\Omega \frac{\partial \rho}{\partial t}\,d\Omega + \int_\Gamma \rho \boldsymbol{q}\cdot\boldsymbol{n}\,ds = 0 \tag{1}$$

Momentum conservation:

$$\int_\Omega \frac{\partial \rho \boldsymbol{q}}{\partial t}\,d\Omega + \int_\Gamma \rho \boldsymbol{q}(\boldsymbol{q}\cdot\boldsymbol{n})\,ds = \int_\Gamma \boldsymbol{\tau}_n\,ds \tag{2}$$

In low-speed combustion, the kinetic energy is negligible comparing with enthalpy, therefore the energy conservation can be simplified as[8]

$$\int_\Omega \frac{\partial(\rho h - p)}{\partial t}\,d\Omega + \int_\Gamma \rho h(\boldsymbol{q}\cdot\boldsymbol{n})\,ds = \int_\Gamma \boldsymbol{\tau}_n\cdot\boldsymbol{q}\,ds + \int_\Gamma \lambda_h(\nabla h\cdot\boldsymbol{n})\,ds \tag{3}$$

Presented as Paper 95-2444 at the AIAA/ASME/SAE/ASEE 31st Joint Propulsion Conference and Exhibit, July 10–12, 1995; received July 31, 1995; revision received March 31, 1996; accepted for publication March 31, 1996.

*Research Associate, Mathematics Department; currently at Louisiana Tech University, Ruston, LA 71272. Member AIAA.

†Assistant Professor, Mathematics Department; currently at Louisiana Tech University, Ruston, LA 71272. Member AIAA.

‡Associate Professor, Mathematics Department; currently at Louisiana Tech University, Ruston, LA 71272. Member AIAA.

Chemical species equation:

$$\int_\Omega \frac{\partial \rho Y_\alpha}{\partial t}\,d\Omega + \int_\Gamma \rho Y_\alpha(\boldsymbol{q}\cdot\boldsymbol{n})\,ds = \int_\Gamma \lambda_Y(\nabla Y_\alpha\cdot\boldsymbol{n})\,ds + \int_\Omega R_\alpha\,d\Omega \qquad \alpha = 1, 2, \ldots, NS \tag{4}$$

Enthalpy and state equations:

$$h = h(Y_\alpha, T) \tag{5}$$

$$p = \sum_\alpha \frac{Y_\alpha}{W_\alpha}\rho RT \tag{6}$$

where t is time, Ω is a fixed control volume with boundary Γ, ρ is density, p is pressure, $\boldsymbol{q}$ is velocity vector, T is temperature, h is enthalpy, $\boldsymbol{n}$ is the unit outer normal vector of the boundary, τ_n is the total viscous stress acted on a surface with outer normal vector $\boldsymbol{n}$, and R_α is the chemical reaction rate of species α. The variables R, Y_α, and W_α are the gas constant, mass fraction, and molecular weight of species α, respectively, and the specific enthalpy and species diffusion coefficients are determined from

$$\lambda_h = [(\mu_C/Pr_L) + (\mu_T/Pr_T)] \tag{7}$$

$$\lambda_Y = [(\mu_C/Sc_L) + (\mu_T/Sc_T)] \tag{8}$$

where μ_C is molecular viscosity, μ_T is the turbulent viscosity determined by turbulence models, Pr_L and Pr_T are the laminar and turbulent Prandtl numbers, respectively, and Sc_L and Sc_T are the laminar and turbulent Schmidt numbers, respectively. From the constitutive relations, we have

$$[\tau] = -(p + \tfrac{2}{3}\mu\nabla\cdot\boldsymbol{q})[I] + 2\mu[\varepsilon] \tag{9}$$

$$\varepsilon_{i,j} = \left[\frac{\partial q_i}{\partial x_j} + \frac{\partial q_j}{\partial x_i}\right] \tag{10}$$

$$\mu = \mu_C + \mu_T \tag{11}$$

Both h and μ can be calculated by the following formulas:

$$h = \sum_\alpha Y_\alpha h_\alpha, \quad h_\alpha = \int_0^T C_{P_\alpha}\,dT_\alpha = h_{0_\alpha} + \int_{T_0}^T C_{P_\alpha}\,dT_\alpha \tag{12}$$

$$C_{P_\alpha} = C^0_{P_\alpha} + C^1_{P_\alpha}T + C^2_{P_\alpha}T^2 + C^3_{P_\alpha}T^3 + C^4_{P_\alpha}T^4 \tag{13}$$

$$\mu_C = \sum_\alpha Y_\alpha\mu_\alpha, \quad \mu_\alpha = \mu^0_\alpha + \mu^1_\alpha T + \mu^2_\alpha T^2 + \mu^3_\alpha T^3 + \mu^4_\alpha T^4 \tag{14}$$

where h_{0_α} is the standard formation enthalpy of the αth species, $C^0_{P_\alpha}, C^1_{P_\alpha}, \ldots, C^4_{P_\alpha}$, $\mu^0_\alpha, \mu^1_\alpha, \ldots, \mu^4_\alpha$ are polynomial coefficients for C_{P_α} and μ_α, respectively.

All thermal and transport parameters are obtained by linking with CHEMKIN-II[15] standard libraries.

III. Chemical Reaction Model

For laminar flames, the chemical reaction rate R_α for the αth species can be calculated by

$$R_\alpha = \omega_\alpha \sum_{j=1}^{N_R}\left[(\nu_{j\alpha} - \hat{\nu}_{j\alpha})\left(F_j\prod_{l=1}^{N_S} n_l^{\hat{\nu}_{jl}} - B_j\prod_{l=1}^{N_S} n_l^{\nu_{jl}}\right)\right] \tag{15}$$

where ω_α is the molecular weight of species α, N_R is the total number of reaction steps, N_S is the total number of species, $\nu_{j\alpha}(\hat{\nu}_{j\alpha})$ refers to the stoichiometric coefficient of products (reactants), and $n_l = \rho Y_l/\omega_l$.

The function $F_j(B_j)$ is the rate constant for the forward (backward) reaction step j. We assume F_j has the following Arrhenius temperature-dependent form:

$$F_j = A_j T^{\alpha_j}\exp[-(E_j/RT)] \tag{16}$$

and B_j has a similar expression. The reverse rate constant can be written in terms of the forward rate constant and the equilibrium constant C_j as

$$B_j = F_j/C_j \tag{17}$$

Here, C_j is also obtained by calling CHEMKIN-II. The pre-exponential factor A_j, the temperature exponent α_j, and the activation energy E_j can be compiled from published experimental work.

For turbulent reacting flows, the algebraic correlation closure (ACC) model is used to introduce a correction term to the reaction rate.[4,5]

IV. Staggered Finite Volume Scheme

One may think that the use of mass fluxes (similar to contravariant velocities) on a staggered grid will result in messy governing equations and cause great difficulties in coding. However, that is not always true. On the other hand, the staggered grid methods have some distinctive features that are very desirable for numerical simulations. The following reasons are why we chose these methods to solve the reacting flow on arbitrary grids:

1) Using a staggered grid can result in more accurate and robust schemes as concluded by numerical analysis and confirmed by our previous calculations on regular Cartesian grids.

2) On a general curvilinear grid system, the staggered grid method can be best used by combining with mass fluxes or contravariant velocities. For each equation of mass fluxes, the discretization stencil for its pressure gradient in the main direction is the most spatially compact, therefore eliminating the possibility of odd–even decoupling of pressure.

3) The use of the mass fluxes also benefits the solution of mass, energy, and chemical species equations. The flow convection is accurately represented.

4) With the use of proper discretization and careful selection of definition locations for variables, the governing equations can be kept simple enough for the momentum equations, and even simpler for all scalar conservation equations.

5) Most importantly, this method will retain the close relation between mass flux and pressure difference on curvilinear grids. Therefore, the pressure-correction method can be used very efficiently. This feature yields a fast convergence on curvilinear grids that is similar to that on Cartesian grids.

In this work, the basic scheme is the finite volume method. The computational domain is discretized into a number of quadrilateral cells in two dimensions or hexahedral cells in three dimensions. As shown in Fig. 1, 1-2-3-4-5-6-7-8 forms a typical cell in three-dimensional problems. In finite volume formulation, the mass fluxes across cell interfaces in each of the three cell index directions can be expressed as

$$\begin{aligned}\rho U_{i+1/2,j,k} &= (\rho\boldsymbol{q}\cdot\boldsymbol{S}_{5678})_{i+1/2,j,k}\\ \rho V_{i,j+1/2,k} &= (\rho\boldsymbol{q}\cdot\boldsymbol{S}_{2376})_{i,j+1/2,k}\\ \rho W_{i,j,k+1/2} &= (\rho\boldsymbol{q}\cdot\boldsymbol{S}_{3487})_{i,j,k+1/2}\end{aligned} \tag{18}$$

where $\boldsymbol{q} = [u, v, w]^T$ is the velocity vector in Cartesian coordinates (x, y, and z), (U, V, and W) are the flow fluxes that are equivalent to the scaled contravariant velocities multiplied

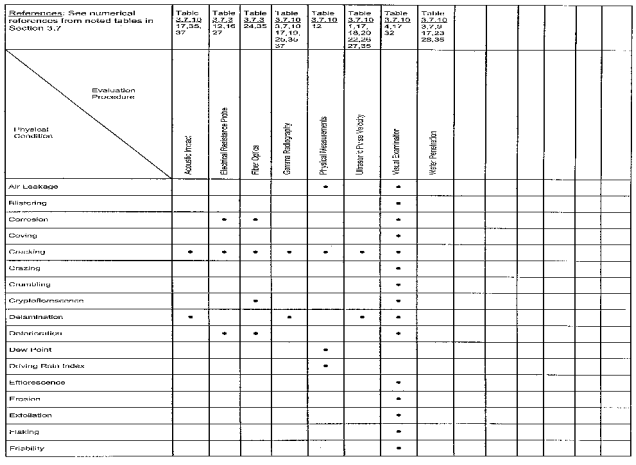

Fig. 1 Control volume and cell surface locations.

by transformation Jacobian, subscripts i, j, and k denote the cell indexes in three curvilinear coordinate directions, respectively.

The cell face vectors are denoted as follows for clarity:

$$\begin{aligned} \boldsymbol{S}^1 &= \boldsymbol{S}_{\xi=\text{const}} = (S^{1x}, S^{1y}, S^{1z}) \\ \boldsymbol{S}^2 &= \boldsymbol{S}_{\eta=\text{const}} = (S^{2x}, S^{2y}, S^{2z}) \\ \boldsymbol{S}^3 &= \boldsymbol{S}_{\zeta=\text{const}} = (S^{3x}, S^{3y}, S^{3z}) \end{aligned} \tag{19}$$

Generally, the velocity fluxes are expressed as

$$\begin{aligned} U &= uS^{1x} + vS^{1y} + wS^{1z} \\ V &= uS^{2x} + vS^{2y} + wS^{2z} \\ W &= uS^{3x} + vS^{3y} + wS^{3z} \end{aligned} \tag{20}$$

$$\begin{bmatrix} u \\ v \\ w \end{bmatrix} = A \begin{bmatrix} U \\ V \\ W \end{bmatrix}, \qquad A = \begin{bmatrix} S^{1x} & S^{1y} & S^{1z} \\ S^{2x} & S^{2y} & S^{2z} \\ S^{3x} & S^{3y} & S^{3z} \end{bmatrix}^{-1} \tag{21}$$

For simplicity, Eq. (21) is denoted as

$$q_l = a_{lm} U^m \tag{22}$$

which will be referred to frequently later in this paper.

In the actual computation, ρU, ρV, and ρW are regarded as the dependent variables instead of U, V, and W. The reasons for this are twofold. First, they are conservative quantities. The advantage becomes obvious in combustion simulation. During the early stage of iteration, temperature may change significantly from step to step when ignition is started or the flame is expanding. Therefore the density will change greatly as well. If U, V, and W are used as dependent variables, the mass conservation will be totally lost after the energy equation is solved and the density is updated since the mass flux ρU, ρV, and ρW will also change as density changes. On the other hand, if ρU, ρV, and ρW are used as the dependent variables, obtained only from the momentum equation and mass equation, they will not change even if a new density field is obtained from the solution of the energy equation. And so, the mass conservation is still kept. That makes the iteration quite robust and very efficient. Secondly, the resulting equations are relatively simpler. This is apparent if the viscous terms are not considered. It is true the viscous terms will be more complicated since viscous stresses are only involved with velocity derivatives. However, the complication of viscous terms can be easily removed in actual programming by introducing a temporal array to store $\rho U/\rho$, $\rho V/\rho$, and $\rho W/\rho$ before viscous force is calculated.

The variable ρU is defined at $(i + \frac{1}{2}, j, k)$; ρV is defined at $(i, j + \frac{1}{2}, k)$; and ρW is defined at $(i, j, k + \frac{1}{2})$. All other variables, ρ, p, h, and Y_α, are defined at the call centers. Only ρ, ρU, ρV, ρW, h, and Y_α are the dependent variables that are solved directly from the integral conservation Eqs. (1–4). All other parameters are determined from relations (5–10).

The governing equations for the mass fluxes can be established through coordinate transformation, then their forms are indeed quite complicated. Karki and Patankar[16] use the velocity components along the grid line as the dependent variables in momentum equations. The discretization equations for these velocity components are obtained using an algebraic manipulation of the discretization equations for the Cartesian velocity components to avoid complicated tensor algebra. This approach has also been successfully used by the present authors in developing a high-order scheme for direct numerical simulation.[17] But we prefer using the contravariant velocities (or mass flux) instead of the velocity components along the grid line, because the mass equation can be expressed straightforwardly by the contravariant velocities, and the resulting pressure-correction equation is simpler.

For highly compressible flows, conservation is strongly emphasized, especially when there are discontinuities in the solution, like shock wave in transonic flow and flame front in combustion. To correctly capture the location of discontinuity in the flowfield, strongly conservative schemes must be used. In the aforementioned approach,[16,17] the geometric terms from grid stretch, curvature, and skewness are majorly presented as source terms in the discretization equations. It is really hard to ensure conservation for these terms.

In this article, the integral form of the governing equations is used. All of the geometric parameters together with flow variables are put in a flux form, which measures the transaction of mass, momentum, and energy across the control volume interfaces. In this way, local balance, as well as global conservation, will be guaranteed once the solution is converged.

The discretization equations for mass fluxes are obtained by applying the momentum equation to certain control volumes with finite volume techniques. For example, the equation for $\rho U_{i+1/2,j,k}$ can be obtained by simply multiplying Eq. (2) with the face vector $\boldsymbol{S}^1_{i+1/2,j,k}$, and applied to control volume $Vol_{i+1/2,j,k}$, which is formed by connecting ξ-line midpoint abcdhefg as shown in Fig. 1:

$$\int_{\Omega_U} \frac{\partial \rho(\boldsymbol{q}\cdot\boldsymbol{S}^1)}{\partial t}\,\mathrm{d}\Omega + \int_{\Gamma_U} \rho(\boldsymbol{q}\cdot\boldsymbol{S}^1)(\boldsymbol{q}\cdot\boldsymbol{n})\,\mathrm{d}s = \int_{\Gamma_U} \boldsymbol{S}^1\cdot\boldsymbol{\tau}_n\,\mathrm{d}s \tag{23}$$

This equation represents the momentum conservation in direction of $\boldsymbol{S}^1$. Keep in mind that $\boldsymbol{S}^1 = \boldsymbol{S}^1_{i+1/2,j,k}$ is a constant vector within the control volume $\Omega_U = Vol_{i+1/2,j,k}$, but it changes from control volume to control volume.

In the previous equation, all $\boldsymbol{q}$ will eventually be expressed in terms of U, V, and W by using Eqs. (20) and (21). We prefer to do the transformation later in the succeeding sections because it will be much easier to do that after discretization.

The momentum equations for ρV and ρW can be obtained similarly.

All of the other equations, i.e., mass conservation, energy conservation, and species equations, are applied to control volume $Vol_{i,j,k}$. They can be put in a general form:

$$\int_\Omega \frac{\partial \rho\phi}{\partial t}\,\mathrm{d}\Omega + \int_\Gamma \rho\phi(\boldsymbol{q}\cdot\boldsymbol{n})\,\mathrm{d}s = \int_\Gamma \lambda(\nabla\phi\cdot\boldsymbol{n})\,\mathrm{d}s + \int_\Gamma F\,\mathrm{d}s + \int_\Omega S\,\mathrm{d}s \tag{24}$$

where $\phi = [1, h, Y_\alpha]^T$, $F = [0, \boldsymbol{\tau}_n\cdot\boldsymbol{q}, 0]^T$, and $S = [0, 0, R_\alpha]^T$ with $\alpha = 1, 2, \ldots, NS$.

The previous equations are not their final forms, the Cartesian velocity $\boldsymbol{q}$ is still used for simplicity. It will be replaced

by mass fluxes during the discretization process described later.

A. Momentum Equations

The ρU Eq. (23) is applied to the staggered control volume $Vol_{i+1/2,j,k}$, and discretized by using the finite volume method as

$$Vol_{i+1/2,j,k}\frac{(\rho U)^{n+1}_{i+1/2,j,k} - (\rho U)^{n}_{i+1/2,j,k}}{\Delta t} + \sum_{l=1}^{6}([\boldsymbol{S}^1\cdot(\rho\boldsymbol{q})]_l)(\boldsymbol{q}\cdot\boldsymbol{S})_l = Vis_{\rho U} \tag{25}$$

where l is the cell surface index, ranging all six cell surfaces of the control volume $Vol_{i+1/2,j,k}$. $Vis_{\rho U}$ is the total viscous stress component in $\boldsymbol{S}^1_{i+1/2,j,k}$ direction acted on the boundary surface of $Vol_{i+1/2,j,k}$ (see Refs. 18 and 19).

By using Eq. (18), the previous formula can be expressed in term-by-term as

$$\begin{aligned} &Vol_{i+1/2,j,k}\frac{(\rho U)^{n+1}_{i+1/2,j,k} - (\rho U)^{n}_{i+1/2,j,k}}{\Delta t} \\ &+ \{\boldsymbol{q}_{i+1,j,k}\cdot\boldsymbol{S}^1_{i+1/2,j,k}\}(\rho U)_{i+1,j,k} - \{\boldsymbol{q}_{i,j,k}\cdot\boldsymbol{S}^1_{i+1/2,j,k}\}(\rho U)_{i,j,k} \\ &+ \{(\rho\boldsymbol{q})_{i+1/2,j+1/2,k}\cdot\boldsymbol{S}^1_{i+1/2,j,k}\}(V)_{i+1/2,j+1/2,k} \\ &- \{(\rho\boldsymbol{q})_{i+1/2,j-1/2,k}\cdot\boldsymbol{S}^1_{i+1/2,j,k}\}(V)_{i+1/2,j-1/2,k} \\ &+ \{(\rho\boldsymbol{q})_{i+1/2,j,k+1/2}\cdot\boldsymbol{S}^1_{i+1/2,j,k}\}(W)_{i+1/2,j,k+1/2} \\ &- \{(\rho\boldsymbol{q})_{i+1/2,j,k-1/2}\cdot\boldsymbol{S}^1_{i+1/2,j,k}\}(W)_{i+1/2,j,k-1/2} = Vis_{\rho U} \end{aligned} \tag{26}$$

Since $\boldsymbol{S}^1$ changes from point-to-point, some terms in Eq. (26), like $(\rho\boldsymbol{q})_{i+1/2,j+1/2,k}\cdot\boldsymbol{S}^1_{i+1/2,j,k}$ cannot be written directly as mass fluxes. But they can be expressed as functions of the mass fluxes by using Eq. (22). For example, $(\rho\boldsymbol{q})_{i+1/2,j+1/2,k}\cdot\boldsymbol{S}^1_{i+1/2,j,k}$ should not be mixed up with $(\rho U)_{i+1/2,j+1/2,k}$; its exact form can be found:

$$\begin{aligned} (\rho\boldsymbol{q})_{i+1/2,j+1/2,k}\cdot\boldsymbol{S}^1_{i+1/2,j,k} &= \{\rho a_{lm}U^m\}_{i+1/2,j+1/2,k}\{S^1_l\}_{i+1/2,j,k} \\ &= \{a_{l1}\}_{i+1/2,j+1/2,k}\{S^1_l\}_{i+1/2,j,k}\{\rho U\}_{i+1/2,j+1/2,k} \\ &\quad + \{a_{l2}\}_{i+1/2,j+1/2,k}\{S^1_l\}_{i+1/2,j,k}\{\rho V\}_{i+1/2,j+1/2,k} \\ &\quad + \{a_{l3}\}_{i+1/2,j+1/2,k}\{S^1_l\}_{i+1/2,j,k}\{\rho W\}_{i+1/2,j+1/2,k} \end{aligned} \tag{27}$$

Based on the idea of the MUSCL scheme, a partially upwind-biased scheme is developed to approximate the momentum fluxes through cell surfaces. The basic idea is that the flux through the control volume surface is regarded as the product of the mass flow and the conserved quantity. According to the sign of mass flux, the conserved quantity is set to its upwind-side value. Thanks to the staggered scheme, the mass flux through the surfaces is always directly available. There are only two possible locations for all of the control volume surfaces, either the surface lies along with one of the original grid surfaces or it runs through the original grid cell center. In the former case, the mass flux is already defined. In the latter case, since the Cartesian velocity and density are defined at the cell center, the mass flow also can be found straightforwardly. Therefore, only the conserved quantity at the surface needs to be interpolated or obtained through reconstruction of data from the cell-averaged values like van Leer's MUSCL method. This feature ensures that the calculated flux is continuous when mass flow changes sign. For example, if the flux $\boldsymbol{F}$ through a control volume surface $\boldsymbol{S}$ in the i direction consists of mass flow $\boldsymbol{M}$ and the conserved quantity ψ, then

$$\begin{aligned} \boldsymbol{F}_i &= (\boldsymbol{M}\cdot\boldsymbol{S})_i\psi_i \\ &= (\boldsymbol{M}\cdot\boldsymbol{S})^+_i\psi_{i(-)} + (\boldsymbol{M}\cdot\boldsymbol{S})^-_i\psi_{i(+)} \end{aligned} \tag{28}$$

In the previous equation, the superscripts + and − on a variable denote the positive and negative part of the variable, respectively,

$$m^+ = \max(m, 0), \qquad m^- = \min(m, 0) \tag{29}$$

and the superscripts (+) and (−) on an index indicate that the variable is taking the limit value on the interface from the left or the right, respectively. For instance, in i direction we have

$$\psi_{i(-)} = \lim_{\substack{l<i\\ l\to i}}\psi_l, \quad \psi_{i(+)} = \lim_{\substack{l>i\\ l\to i}}\psi_l \tag{30}$$

High-resolution schemes up to third order can be constructed by setting

$$\psi_{i(-)} = \psi_{i-1/2} + \frac{\sigma^{\psi}_{i-1/2}}{4}[(1-\kappa)\nabla + (1+\kappa)\Delta]\psi_{i-1/2}$$

$$\psi_{i(+)} = \psi_{i+1/2} - \frac{\sigma^{\psi}_{i+1/2}}{4}[(1+\kappa)\nabla + (1-\kappa)\Delta]\psi_{i+1/2}$$

where ∇ and Δ are backward- and forward-difference operators and κ is a parameter used to control the order of the scheme. The term $\kappa = (1/3)$ is used in the present method to construct the third-order scheme. When $\kappa = -1$ the scheme degrades to the second-order fully upwind method. The limiter σ is adopted to ensure the monotone interpolation following Koren[20] as

$$\sigma^{\psi}_{l-1/2} = \frac{3\nabla\psi_{l-1/2}\Delta\psi_{l-1/2} + \theta}{2(\nabla\psi_{l-1/2} - \Delta\psi_{l-1/2})^2 + 3\nabla\psi_{l-1/2}\Delta\psi_{l-1/2} + \theta} \tag{31}$$

where a small constant θ with a typical value of 10^{-20} is added to prevent division by zero.

In our solution algorithm, only $(\rho U)_{i+3/2,j,k}$, $(\rho U)_{i-1/2,j,k}$, $(\rho U)_{i+1/2,j+1,k}$, $(\rho U)_{i+1/2,j-1,k}$, $(\rho U)_{i+1/2,j,k+1}$, $(\rho U)_{i+1/2,j,k-1}$, $(\rho U)_{i+1/2,j,k}$, $p_{i,j,k}$, and $p_{i+1,j,k}$ are treated implicitly for ρU equation. In general, the ρU equation can be expressed in δ form as

$$\begin{aligned} &A_E\delta(\rho U)_{i+3/2,j,k} + A_W\delta(\rho U)_{i-1/2,j,k} + A_N\delta(\rho U)_{i+1/2,j+1,k} \\ &+ A_S\delta(\rho U)_{i+1/2,j-1,k} + A_F\delta(\rho U)_{i+1/2,j,k+1} \\ &+ A_B\delta(\rho U)_{i+1/2,j,k-1} + A_C\delta(\rho U)_{i+1/2,j,k} + A^p_L\delta p_{i,j,k} \\ &+ A^p_R\delta p_{i+1,j,k} = -Ru_{i+1/2,j,k} \end{aligned} \tag{32}$$

where Ru denotes the residual of ρU equation, including convection and diffusion terms.

Similarly, the momentum equations of ρV and ρW can be found.

B. Scalar Conservation Equations

All of the scalar conservation Eq. (24) is discretized in control volume $Vol_{i,j,k}$ with cell-centered finite volume scheme. The previous upwind-biased scheme with limiter is used for the convection terms. The second-order compact central difference scheme is used for the diffusion terms. The only exception is the mass conservation equation, which benefits most from the staggered grid. The discretized equation has the sim-

plest form and is the most compact in space in terms of mass fluxes

$$\delta(\rho U)_{i+1/2,j,k} - \delta(\rho U)_{i-1/2,j,k} + \delta(\rho V)_{i,j+1/2,k} - \delta(\rho V)_{i,j-1/2,k} + \delta(\rho W)_{i,j,k+1/2} - \delta(\rho W)_{i,j,k-1/2} = -Rm_{i,j,k} \tag{33}$$

where $\delta(\ ) = (\ )^{n+1} - (\ )^n$, and

$$Rm_{i,j,k} = Vol\,\frac{\rho^{n+1}_{i,j,k} - \rho^n_{i,j,k}}{\Delta t} + (\rho U)^n_{i+1/2,j,k} - (\rho U)^n_{i-1/2,j,k} + (\rho V)^n_{i,j+1/2,k} - (\rho V)^n_{i,j-1/2,k} + (\rho W)^n_{i,j,k+1/2} - (\rho W)^n_{i,j,k+1/2}$$

In case only steady state is interested, the time-dependent term of mass equation can be dropped for fast convergence.

All other equations are discussed in their general form [Eq. (24)] except for the source term and the stress work term. The source terms of the species equations are usually dominant and strongly nonlinear. We will discuss the treatment of those source terms in Sec. IV.C. The stress work term in the energy equation has no contribution to the implicit coefficients, its discretization form can be found in Refs. 18 and 19. If we leave the implicit coefficients contributed by the source terms to Sec. IV.C, the discretized forms of Eq. (24) can be written in the following form:

$$\Phi_E\delta\phi_{i+1,j,k} + \Phi_W\delta\phi_{i-1,j,k} + \Phi_N\delta\phi_{i,j+1,k} + \Phi_S\delta\phi_{i,j-1,k} + \Phi_F\delta\phi_{i,j,k+1} + \Phi_B\delta\phi_{i,j,k-1} + \Phi_C\delta\phi_{i,j,k} = -Res(\phi) \tag{34}$$

where $Res(\phi)$ is the residual of ϕ equation.

The convection term is discretized by using the same method described in Sec. IV.B. The diffusion term on the right side of Eq. (24) is discretized through two steps. First we calculate the gradient $\nabla\phi$ on the cell surface by applying Gauss's formula to the respective staggered control volume, and then assemble the integration. Since the gradients are computed locally, the resulting scheme reduces to a compact one when the regular grid is used.

C. Implicit Treatment of Reaction Source Term

The major difficulty in the calculation of finite rate combustion is the stiffness of the species equations. To solve this problem, the source terms (production rate of chemical reaction) must be treated implicitly.

In Sec. IV.B, the discretization of time-dependent, convection, and diffusion terms of the general scalar conservation equation is discussed. For the chemical species equations, the discretized equations can be written as

$$\Phi_E\delta Y_{\alpha_{i+1,j,k}} + \Phi_W\delta Y_{\alpha_{i-1,j,k}} + \Phi_N\delta Y_{\alpha_{i,j+1,k}} + \Phi_S\delta Y_{\alpha_{i,j-1,k}} + \Phi_F\delta Y_{\alpha_{i,j,k+1}} + \Phi_B\delta Y_{\alpha_{i,j,k-1}} + \Phi_C\delta Y_{\alpha_{i,j,k}} = -[C_T(Y_\alpha)^n - D_T(Y_\alpha)^n - R_\alpha] \tag{35}$$

where C_T is the convection term and D_T is the diffusion term. R_α is the reaction rate defined in Eq. (15):

$$R_\alpha = W_\alpha \sum_{m=1}^{N_R} \left\{ (\nu_{m\alpha} - \hat{\nu}_{m\alpha}) \left[F_m \prod_{l=1}^{N_S} \left(\frac{\rho Y_l}{W_l}\right) \hat{\nu}_{ml} - B_m \prod_{l=1}^{N_S} \left(\frac{\rho Y_l}{W_l}\right) \nu_{ml} \right] \right\}$$

The reaction rate is usually very large and dominant near the flame front. Therefore, implicit treatment for the reaction rate term is necessary. Using Taylor expansion, we have

$$R^{n+1}_\alpha = R^n_\alpha + \sum_l \frac{\partial R_\alpha}{\partial Y_l}\,\delta Y_l + \sum_l \mathbb{O}(\delta Y_l^2) \tag{36}$$

Defining

$$R = (R_1, R_2, \ldots, R_{N_S})^T$$

$$\delta Y = (\delta Y_1, \delta Y_2, \ldots, \delta Y_{N_S})^T$$

$$D_{\alpha l} = \frac{\partial R_\alpha}{\partial Y_l}$$

we may have

$$R^{n+1} \approx R^n + D\delta Y \tag{37}$$

where D is an N_S by N_S matrix.

It is apparent that the implicit treatment of R_α requires a coupled solution of all species equations. By denoting

$$Res_\alpha = C_T(Y_\alpha)^n - D_T(Y_\alpha)^n - R^n_\alpha \tag{38}$$

for the residual of the αth species equation, and

$$Res = (Res_1, Res_2, \ldots, Res_{N_S})^T \tag{39}$$

for the residual vector, Eq. (35) becomes

$$\Phi_E I\delta Y_{i+1,j,k} + \Phi_W I\delta Y_{i-1,j,k} + \Phi_N I\delta Y_{i,j+1,k} + \Phi_S I\delta Y_{i,j-1,k} + \Phi_F I\delta Y_{i,j,k+1} + \Phi_B I\delta Y_{i,j,k-1} + (\Phi_C I + D)\delta Y_{i,j,k} = -Res \tag{40}$$

where I is a unit matrix with the elements

$$I_{lm} = \begin{cases} 0 & \text{if } l \neq m \\ 1 & \text{if } l = m \end{cases} \tag{41}$$

and Φ is a scalar.

Equation (40) is the final form of the species equations. They are solved in a coupled way. If line relaxation is used along the j line and the Gauss–Seidel iteration is used in i, k directions, for instance, then Eq. (40) can be rewritten as

$$\Phi_S I\delta Y^{\text{new}}_{i,j-1,k} + (\Phi_C I + D)\delta Y^{\text{new}}_{i,j,k} + \Phi_N I\delta Y^{\text{new}}_{i,j+1,k} = -Res - \Phi_E I\delta Y^{\text{old}}_{i+1,j,k} - \Phi_W I\delta Y^{\text{new}}_{i-1,j,k} - \Phi_F I\delta Y^{\text{old}}_{i,j,k+1} - \Phi_B I\delta Y^{\text{new}}_{i,j,k-1} \tag{42}$$

The left-hand side of Eq. (42) forms a block–tridiagonal system, which can be solved by using the tailor-made algorithm combined with a Gauss elimination method for the small block matrix inversion.

V. Computational Procedures

To solve the governing equations discretized in foregoing sections, an implicit time-marching method has been developed. The governing equations are divided into two sets: 1) the flow part and 2) the chemical reaction part. They are solved alternately to avoid solving a huge system of equations at the same time. Different solving techniques are applied to those two sets of equations.

In the laminar case, the system consists of 21 equations (if there are 16 species). In the turbulent case, there will be 23 equations. They are solved in groups: 1) ρU, ρV, ρW, and p by solving the mass and momentum equations; 2) k, ε, and μ_t by solving the turbulence model in turbulent combustion case; 3) h, and Y_α by solving the energy and species equations; and finally, updating 4) ρ and μ by calling CHEMKIN-II.

For the flow part, a line-distribution updating scheme[21,22] is used. To further accelerate the convergence, a semicoarsening multigrid method is developed. Here we only describe the techniques we used for our specific applications. In our

method, the density and pressure are defined at the cell center and the contravariant velocities are defined at cell interfaces. The density and pressure are transferred from the finer level by area weighting to the coarser grid; the contravariant velocities on coarser grid are simply set to be the sum of those at corresponding interfaces. The residuals on finer grids are restricted to coarser by adding up the corresponding part to the staggered stencils. After relaxation is completed on the coarser grid, the corrections are fed back to the finer grid by bilinear interpolation.

For the reaction part, the energy equation is solved together with the species equations. An implicit alternate line-relaxation method is used for the energy equation. The species equations are treated in a fully coupled way. The reaction source terms, which are non-linear and usually troublesome, are treated implicitly through linearization. The block–line tridiagonal solver combined with vectorized pivoting Gauss elimination is used, which was found very effective to handle the sensitivity and stiffness of the system.

The multigrid method is used only for momentum and continuity equations in this work. The other equations, such as energy equation, species equations and κ, ε equations, are solved on a single grid. Therefore, we cannot achieve full multigrid efficiency. However, the whole process for solving our system is still substantially accelerated.

VI. Boundary Conditions

The boundary type usually encountered can be classified as inflow, outflow, solid wall, symmetrical (slip), and periodical. At the inflow boundary, the flow velocity, enthalpy, and chemical species are specified, but the pressure is extrapolated from the interior, then the density is found by using the state equation.

For the outflow boundary, the back pressure is prescribed and other variables are extrapolated from the interior.

For the solid wall boundary, since a ghost cell is always introduced, both slip (symmetrical) and nonslip conditions can be easily implemented with use of mass fluxes. The idea can be shown by considering wall conditions on a j = const plane. For nonslip conditions, reverse reflection is applied to all of the mass fluxes associated with the ghost cell. For a slip (symmetrical) boundary, the reverse reflection is only applied to V, direct reflection is applied to U and V. In both cases, the velocity flux V lying on this plane (j = const) is always set to zero.

Table 1 C_1–chain methane–air reaction mechanism[a]

No.	Reaction	A	α	E
1	$CH_3 + H \rightleftharpoons CH_4$	1.90E+36	−7	9050
2	$CH_4 + O_2 \rightleftharpoons CH_3 + HO_2$	7.90E+13	0	56,000
3	$CH_4 + H \rightleftharpoons CH_3 + H_2$	2.20E+4	3	8750
4	$CH_4 + O \rightleftharpoons CH_3 + OH$	1.60E+6	2.36	7400
5	$CH_4 + OH \rightleftharpoons CH_3 + H_2O$	1.60E+6	2.1	2460
6	$CH_2O + OH \rightleftharpoons HCO + H_2O$	7.53E+12	0	167
7	$CH_2O + H \rightleftharpoons HCO + H_2$	3.31E+14	0	10,500
8	$CH_2O + M \rightleftharpoons HCO + H + M$	3.31E+16	0	81,000
9	$CH_2O + O \rightleftharpoons HCO + OH$	1.81E+13	0	3082
10	$HCO + OH \rightleftharpoons CO + H_2O$	5.00E+12	0	0
11	$HCO + M \rightleftharpoons H + CO + M$	1.60E+14	0	14,700
12	$HCO + H \rightleftharpoons CO + H_2$	4.00E+13	0	0
13	$HCO + O \rightleftharpoons OH + CO$	1.00E+13	0	0
14	$HCO + O_2 \rightleftharpoons HO_2 + CO$	3.00E+12	0	0
15	$CO + O + M \rightleftharpoons CO_2 + M$	3.20E+13	0	−4200
16	$CO + OH \rightleftharpoons CO_2 + H$	1.51E+7	1.3	−758
17	$CO + O_2 \rightleftharpoons CO_2 + O$	1.60E+13	0	41,000
18	$CH_3 + O_2 \rightleftharpoons CH_3O + O$	7.00E+12	0	25,652
19	$CH_3O + M \rightleftharpoons CH_2O + H + M$	2.40E+13	0	28,812
20	$CH_3O + H \rightleftharpoons CH_2O + H_2$	2.00E+13	0	0
21	$CH_3O + OH \rightleftharpoons CH_2O + H_2O$	1.00E+13	0	0
22	$CH_3O + O \rightleftharpoons CH_2O + OH$	1.00E+13	0	0
23	$CH_3O + O_2 \rightleftharpoons CH_2O + HO_2$	6.30E+10	0	2600
24	$CH_3 + O_2 \rightleftharpoons CH_2O + OH$	5.20E+13	0	34,574
25	$CH_3 + O \rightleftharpoons CH_2O + H$	6.80E+13	0	0
26	$CH_3 + OH \rightleftharpoons CH_2O + H_2$	7.50E+12	0	0
27	$HO_2 + CO \rightleftharpoons CO_2 + OH$	5.80E+13	0	22,934
28	$H_2 + O_2 \rightleftharpoons 2OH$	1.70E+13	0	47,780
29	$OH + H_2 \rightleftharpoons H_2O + H$	1.17E+9	1.3	3626
30	$H + O_2 \rightleftharpoons OH + O$	2.20E+14	0	16,800
31	$O + H_2 \rightleftharpoons OH + H$	1.80E+10	1	8826
32	$H + O_2 + M \rightleftharpoons HO_2 + M$[b]	2.10E+18	−1	0
33	$H + O_2 + O_2 \rightleftharpoons HO_2 + O_2$	6.70E+19	−1.42	0
34	$H + O_2 + N_2 \rightleftharpoons HO_2 + N_2$	6.70E+19	−1.42	0
35	$OH + HO_2 \rightleftharpoons H_2O + O_2$	5.00E+13	0	1000
36	$H + HO_2 \rightleftharpoons 2OH$	2.50E+14	0	1900
37	$O + HO_2 \rightleftharpoons O_2 + OH$	4.80E+13	0	1000
38	$2OH \rightleftharpoons O + H_2O$	6.00E+8	1.3	0
39	$H_2 + M \rightleftharpoons H + H + M$[c]	2.23E+12	0.5	92,600
40	$O_2 + M \rightleftharpoons O + O + M$	1.85E+11	0.5	95,560
41	$H + OH + M \rightleftharpoons H_2O + M$	7.50E+23	−2.6	0
42	$H + HO_2 \rightleftharpoons H_2 + O_2$	2.50E+13	0	700
43	$HO_2 + HO_2 \rightleftharpoons H_2O_2 + O_2$	2.00E+12	0	0
44	$H_2O_2 + M \rightleftharpoons OH + OH + M$	1.30E+17	0	45,500
45	$H_2O_2 + OH \rightleftharpoons H_2O + HO_2$	1.00E+13	0	1800

[a]Rate coefficients: $K = AT^{\alpha} \exp(-E/RT)$, units: moles, cubic centimeters, seconds, Kelvins, and calories.

Third body efficiency with respect to Ar:

[b]$H_2O = 21$, $H_2 = 3.3$, $CO = 2.0$, $CO_2 = 5.0$, $N_2 = O_2 = 0$.

[c]$H_2O = 6$, $H = 2$, $H_2 = 3$.

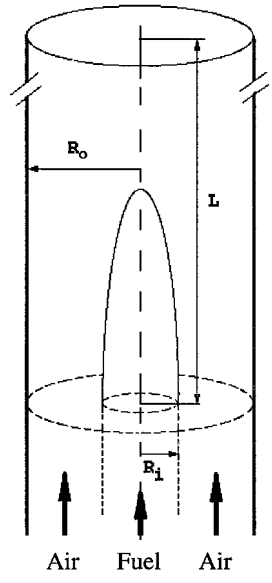

Fig. 2 Schematic configuration of a coflowing burner.

The periodical boundary is the simplest one. All of the values on the ghost cell are taken directly from the corresponding cell on the other side.

All of the boundary conditions are treated implicitly through modification of the implicit coefficients of the discretized equations at the boundary points.

VII. Numerical Results

For a given combustion problem, the chemical reaction mechanism needs to be specified first. The chemical reaction mechanism can be obtained from published experimental work. In the numerical simulation, it is represented by the preexponential factor A_j, the temperature exponent α_j, and the activation energy E_j of the chemical reaction equations. Those parameters and reaction equations are specified through an input data file mech provided by users in our code. In our test cases involving methane–air reaction, the C_1-chain reaction mechanism in Table 1 given by Xu et al.[3] is adopted, in which 16 species are involved in a 45-step reaction chain. Thermal and transport parameters are obtained by calling CHEMKIN-II subroutines and databases.

The first test case is a laminar diffusion flame anchored on

References: See Section 3.7 and Table 3.7.10	12	12													
Evaluation Procedure / Physical Condition	Physical Measurements	Visual Examination													
Bowing	•	•													
Bulging	•	•													
Chipping		•													
Condition of Lintels (Shelf Angles)		•													
Cracking	•	•													
Deflection/Settlement	•	•													
Detachment		•													
Displacement	•	•													
Distortion	•	•													
Plumbness	•	•													
Sagging	•	•													
Spalling		•													
Ties and Anchors		•													
Warping	•	•													

Fig. 3 Axial profiles of a) temperature, b) CH_4, c) O_2, d) H_2O, e) CO_2, and f) N_2 mole fractions along the centerline.

the base of a confined coflow methane–air burner, which was studied experimentally by Mitchell et al.,[23,24] numerically simulated by Smooke et al.,[1,2] and later by Xu et al.[3] Referring to Fig. 2, the physical configuration consists of an inner cylindrical fuel stream with radius $R_i = 0.635$ cm surrounded by a coflowing oxidizer jet (radius $R_0 = 2.54$ cm). The length of the tubular shield $L = 30.0$ cm. The fuel is pure methane (CH_4). The dry air that consists of 23.2% O_2 and 76.8% N_2 in mass fraction is used as the oxidizer. The fuel comes into the burner at a speed of 4.5 cm/s with a temperature of 298 K. The air flows in at a speed of 9.88 cm/s and a temperature of 298 K. The tubular shield is cooled and kept at a constant temperature of 298 K. Since a reverse flow occurred at the exit, and the moisture in the exhaust air is entrained into the burner, special treatment is required at exit boundary conditions. Following the suggestion by Michell,[23] the reverse flow is assumed to consist of 22.8% O_2, 2.11% H_2O, and 75.09% N_2. Since the reverse flow speed is unknown, in our calculation, it is damped down by a factor of 0.8 compared with that of the interior point to stabilize the computation.

As in Xu's et al.[3] calculation, the chemical reaction is assumed to have 15 reactive species and involve 45 steps. In the calculations done by Smooke et al.[1,2] and Xu et al.,[3] the axisymmetric condition was used to reduce the problem into a two-dimensional one. Here we treat this case as a three-dimensional problem. The computational domain covers a quadrant of the cylindrical burner. Since the high-order scheme is used, the results are found very accurate even on a relatively coarse grid of $33 \times 13 \times 17$. As shown in Fig. 3, the predicted axial temperature profile and main species distribution are in excellent agreement with the experimental data. A total of 190 iteration cycles are needed in this case to reduce the maximum residuals of all equations by four orders of magnitude, including 5 cycles for the cold flow, 40 cycles for fast chemical reaction flow, and 145 cycles for finite rate reaction flow calculations. During each iteration cycle, two multigrid V-cycles are performed for the flow part and two iterations for the reaction part. The loose-coupling between these two parts makes the multigrid algorithm work very efficiently for the flowfield, and thus makes the combustion easy to converge. The total CPU time for the calculation is only 210 min on an IBM RS6000/360 workstation.

The second test case is a strong swirling combustion in a three-dimensional gas-turbine combustor. The same fuel as used in the first case enters the combustor through an inner hole with a radius of 1.2 cm. The oxidizer, the air again, flows in coaxially through the outer circular ring with outer radius of 36 cm. Both fuel and air are supposed to pass a swirler before entering the combustor. The inflow velocity profiles are plotted in Fig. 4. The inlet velocity vectors and the combustor configuration are plotted together in Fig. 5. This combustor is simplified from an experimental model.[25] The overall geometrical dimensions are kept the same as the experimental model, but the airjets on the upper and bottom walls are ignored.

Again, the combustion is assumed to have nitrogen and 15 reactive species and involve 45 steps. The calculations are carried out on three different sizes of grids. The computational conditions, grid sizes, convergence, and CPU time are summarized in Tables 2 and 3.

On the coarsest grid, the solution was easily brought to full convergence within 160 steps, including 10 steps for cold-flow calculation, 30 steps for fast reaction, and 120 steps for finite rate reaction steps. The same time steps can reduce the residuals on a middle-size grid ($53 \times 29 \times 29$) by 3.55 orders of magnitude. On the finest mesh, which consists of more than

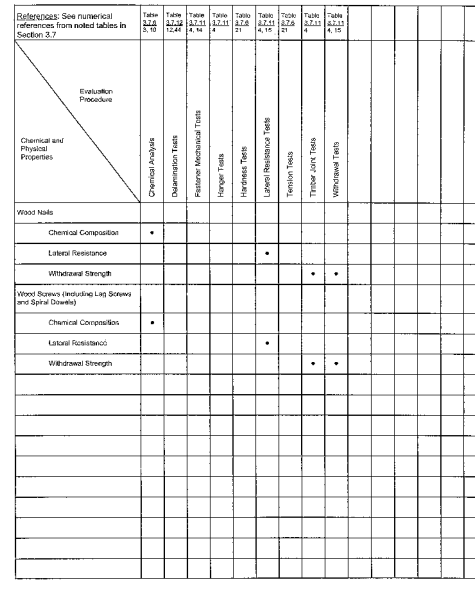

Fig. 4 Combustor inlet velocity profiles.

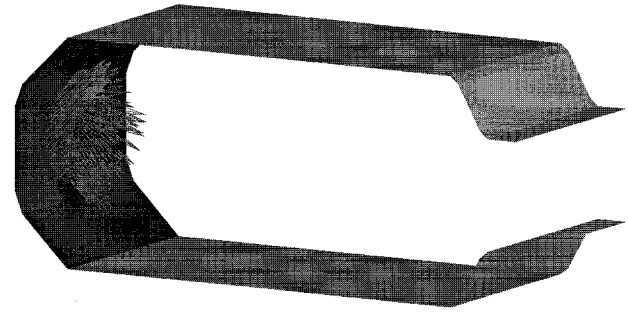

Fig. 5 Velocity vectors at the inlet.

Table 2 Working conditions

Inflow speed	Fuel	Oxidizer	Species number	Reaction steps
See Fig. 5, 45-deg swirling angle	Methane	Air	16	45 (Table 1)

Table 3 Summary of CPU time and convergence on different grids

	Iteration number					
Grid	Cold flow	Fast reaction	Finite rate	Convergence	CPU, h	Machine
$49 \times 21 \times 21$ (21,609)	10	30	120	5.17 orders	1.77	Cray Y-MP
$53 \times 29 \times 29$ (44,573)	10	30	120	3.61 orders	3.57	Cray Y-MP
$49 \times 65 \times 65$ (207,025)	20	30	200	3.30 orders	21.3	Cray Y-MP

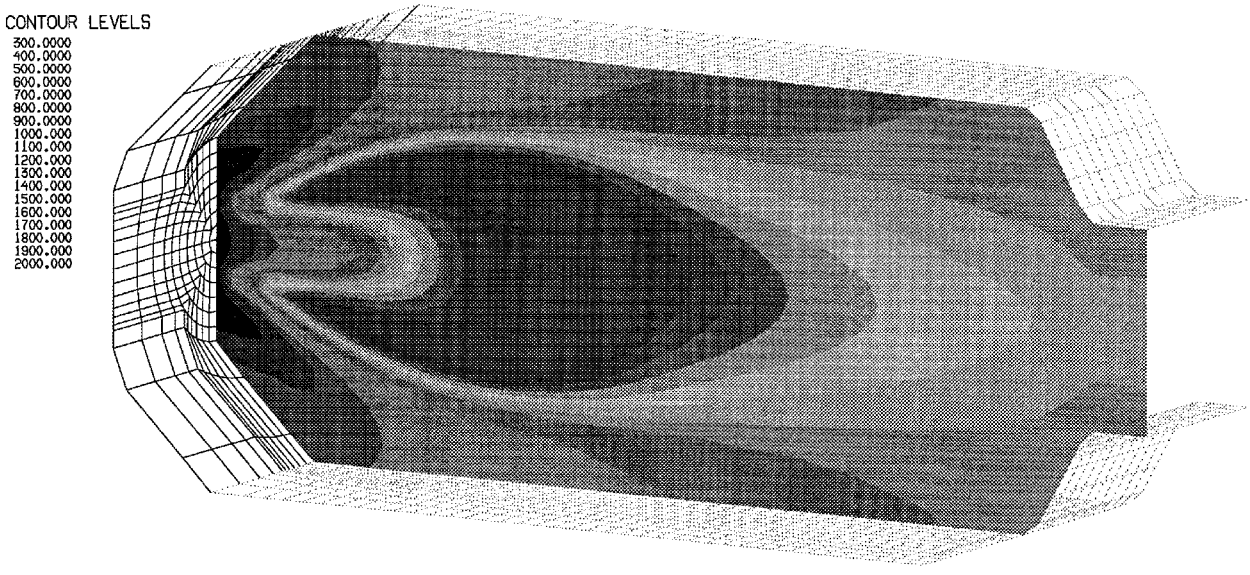

Fig. 6 Temperature isotherms on the center (x, y) plane.

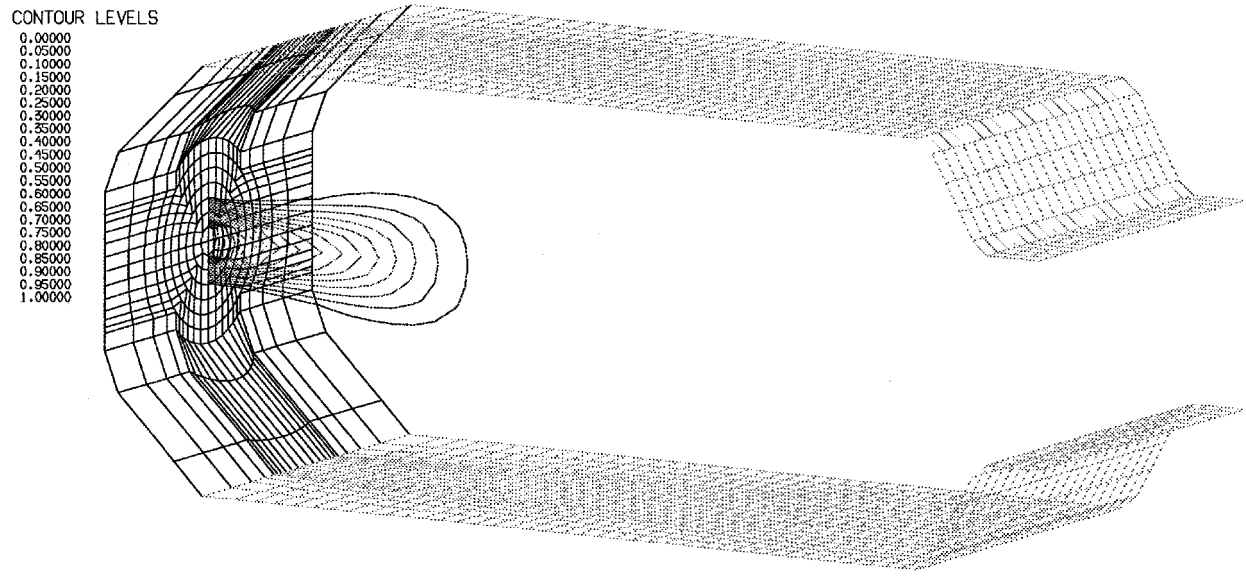

Fig. 7 CH_4 isopleths on the center (x, y) plane.

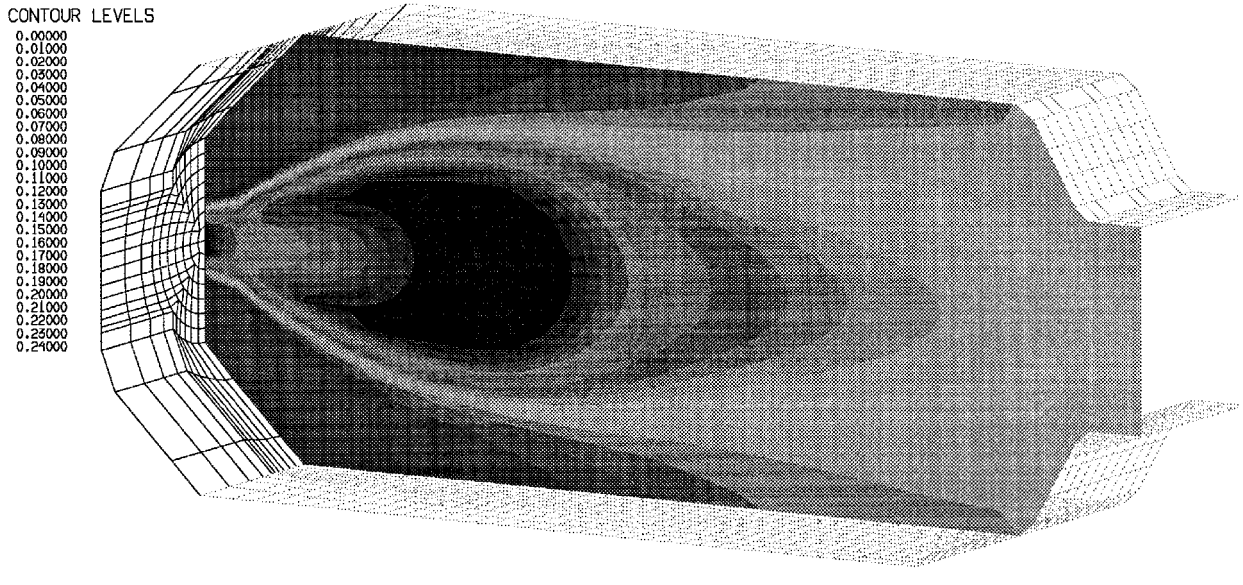

Fig. 8 O_2 isopleths on the center (x, y) plane.

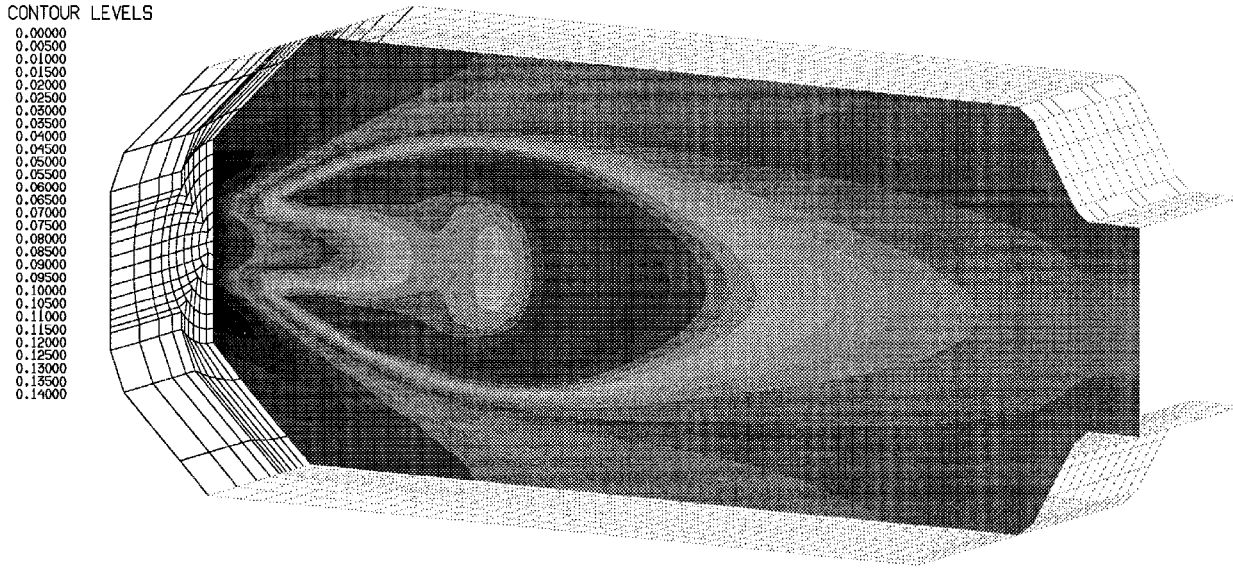

Fig. 9 CO_2 isopleths on the center (x, y) plane.

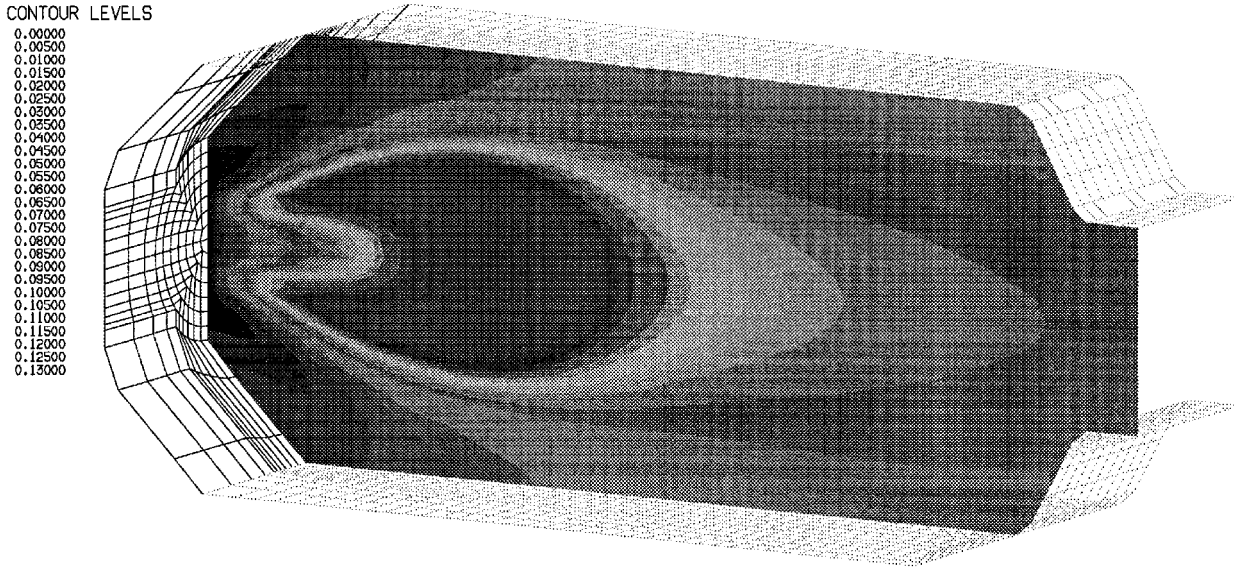

Fig. 10 H_2O isopleths on the center (x, y) plane.

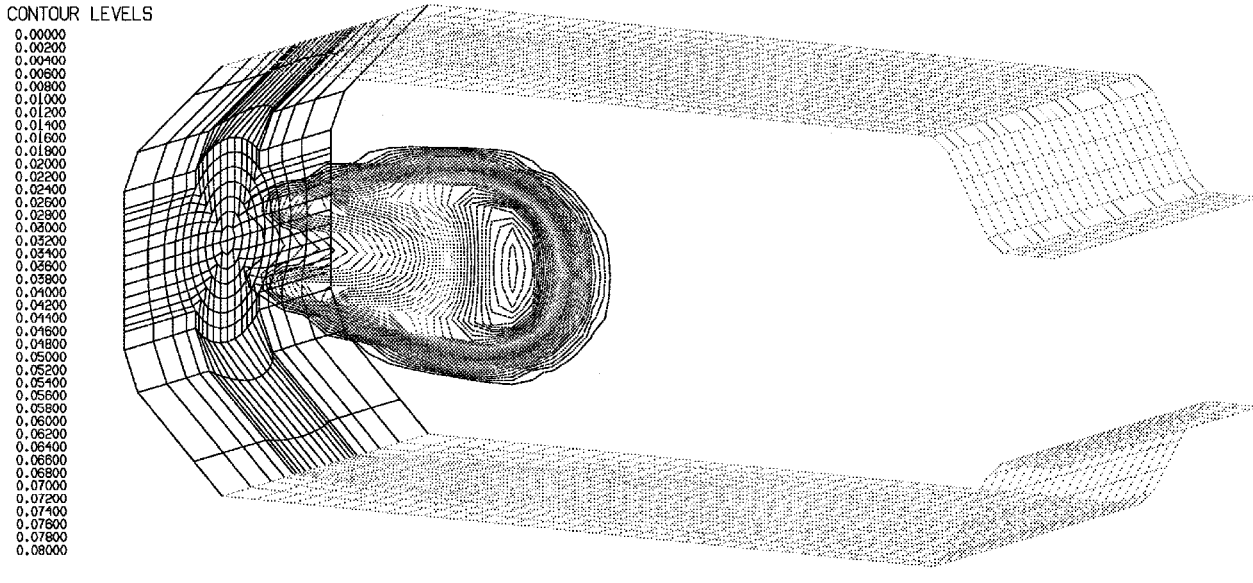

Fig. 11 CO isopleths on the center (x, y) plane.

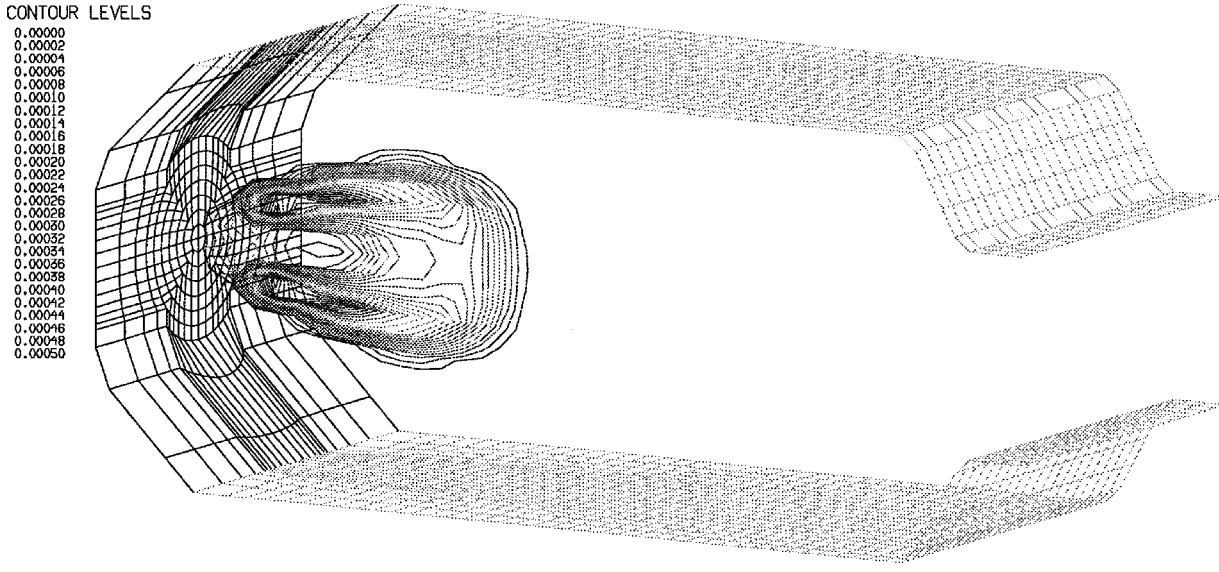

Fig. 12 CH_3 isopleths on the center (x, y) plane.

200,000 grid points, we still have no difficulty making the solution converge, but the solution converges much slower than that on the coarse grid. Eighty more time steps were used in this case to reduce the residuals by 3.21 orders of magnitude. Actually, the results are hardly changed after the residuals were reduced by three orders. The total CPU time for the finest grid computation is about 21 h. Considering the complexity of the flowfield, the large numbers of chemical reactions, and the large size of the grid, the computation is still believed to be very efficient. The successful computation of this case also has a significant meaning, indicating that the simulation of a realistic combustion problem with detailed chemistry is affordable even with present-day computational tools.

Because of space restraints, we only show the results obtained on a middle-size grid. The calculated temperature isotherms on the central plane are plotted in Fig. 6. The mass fraction distributions of main chemical species CH_4, O_2, CO_2, H_2O, CO, and CH_3 are presented in the form of isopleths in Figs. 7–12.

VIII. Conclusions

A highly efficient and accurate method has been developed for calculating general three-dimensional reacting flows with detailed chemistry. A distinctive feature of this method is that the mass fluxes are employed as the dependent variables and they are defined staggeredly at the grid cell surfaces. In this way, the discretization stencils for momentum equations are kept compact in general curvilinear coordinate systems and the possibility of odd–even decoupling of pressure is eliminated.

The use of mass fluxes also benefits the solution of species equations. The flow convection at the cell surfaces of the control volume for species is now accurately represented by the mass fluxes. By taking advantage of the simple wave structures of the species equations, upwind schemes of various orders can be easily constructed based on the local mass fluxes. In the present study, a third-order monotone upwind-biased scheme is used for all convections to minimize numerical diffusion and to capture the sharp gradients existing in flames.

A semicoarsening multigrid method combined with a line-distributive relaxation proves to be a very efficient method for solving the flow equations. Though the multigrid algorithm is only applied to flow part, the whole process of solving the governing system is still substantially accelerated. Since the flowfield acts like the carrier of chemical reaction, it can be easily understood that a fast established flowfield will provide a stable base for the reactions and therefore make the species equations easy to converge. We believe this is the key to greatly reducing the iteration number for the species equations.

The results of coflow diffusion flame calculation demonstrate the accuracy of the present method, while the test case of strong swirling combustion in a gas-turbine combustor shows the capability and efficiency of the present method in modeling real three-dimensional complex combustion with detailed chemistry at an affordable cost.

Acknowledgments

The authors thank NASA Lewis Research Center for the sponsorship of this project. The authors are grateful to John Goodrich at NASA Lewis Research Center for his helpful discussions.

References

[1]Smooke, M. D., Mitchell, R. E., and Keys, D. E., "Numerical Solution of Two Dimensional Axisymmetric Laminar Diffusion Flames," *Combustion Science and Technology*, Vol. 67, 1989, pp. 85–122.

[2]Smooke, M., "Numerical Modeling of Laminar Diffusion Flames," *Numerical Approaches to Combustion Modeling*, edited by E. S. Oran and J. P. Boris, Progress in Astronautics and Aeronautics, AIAA, Washington, DC, 1991, pp. 183–223.

[3]Xu, Y., Smooke, M., Liu, P., and Long, M., "Primitive Variable Modeling of Multidimensional Laminar Flames," *Combustion Science and Technology*, Vol. 90, 1993, pp. 289–313.

[4]Liao, C., Liu, Z., and Liu, C., "Implicit Multigrid Method for Modeling 3-D Turbulent Diffusion Flames with Detailed Chemistry," AIAA Paper 95-0801, Jan. 1995.

[5]Liu, Z., Liao, C., Liu, C., and McCormick, S., "Multigrid Method for Multi-Step Finite Rate Combustion," AIAA Paper 95-0205, Jan. 1995.

[6]Ern, A., Douglas, C. C., and Smooke, M. D., "Detailed Chemistry Modeling of Laminar Diffusion Flames on Parallel Computers," *International Journal of Supercomputer Applications and High Performance Computing*, Vol. 9, No. 3, 1995, pp. 167–186.

[7]Shuen, J. S., "Upwind Differencing and LU Factorization for Chemical Non-Equilibrium Navier-Stokes Equations," *Journal of Computational Physics*, Vol. 99, No. 2, 1992, pp. 233–250.

[8]Bai, X. S., and Fuchs, L., "Calculations of Turbulent Combustion of Propane in Furnaces," *International Journal for Numerical Methods in Fluids*, Vol. 17, No. 3, 1993, pp. 221–239.

[9]Leonard, A. D., and Dai, F., "Application of a Coupled Monte Carlo PDF/Finite Volume CFD Method for Turbulent Combustion," AIAA Paper 94-2904, June 1994.

[10]Chen, K. H., and Shuen, J. S., "Three Dimensional Coupled Implicit Methods for Spray Combustion Flows at All Speeds," AIAA Paper 94-3047, June 1994.

[11]Rizk, N. K., "Calculation Method for NOx Production in Gas

Turbine Combustors,'' AIAA Paper 95-0282, Jan. 1995.

[12]Patankar, S. V., *Numerical Heat Transfer and Fluid Flow*, Hemisphere, Washington, DC, 1980.

[13]Van Leer, B., ''Towards the Ultimate Conservative Difference Scheme V: A Second-Order Sequel to Gudonov's Method,'' *Journal of Computational Physics*, Vol. 32, No. 1, 1979, pp. 101–136.

[14]Anderson, W. K., Thomas, J. L., and Van Leer, B., ''Comparison of Finite Volume Flux Vector Splittings for the Euler Equations,'' *AIAA Journal*, Vol. 24, No. 9, 1986, pp. 1453–1460.

[15]Kee, R. J., Rupley, F. M., and Miller, J. A., ''CHEMKIN-II: A Fortran Chemical Kinetics Package for the Analysis of Gas Phase Chemical Kinetics,'' Sandia National Labs., SAND89-80093, UC-706, Oct. 1989.

[16]Karki, K. C., and Patankar, S. W., ''Pressure Based Calculation Procedure for Viscous Flows at All Speed in Arbitrary Configurations,'' *AIAA Journal*, Vol. 27, No. 9, 1989, pp. 1167–1174.

[17]Liu, Z., Xiong, G., and Liu, C., ''Direct Numerical Simulation for the Whole Process of Transition on 3-D Airfoil,'' AIAA Paper 96-2081, June 1996.

[18]Zheng, X., Liu, C., Liao, C., Liu, Z., and McCormick, S., ''Multigrid Method for Modeling Multi-Dimensional Combustion with Detailed Chemistry,'' Copper Mountain Conf. on Multigrid Methods 1995 (CCMM'95), Dept. of Energy and NASA, Copper Mountain, CO, April 1995.

[19]Zheng, X., and Liu, C., ''A Contravariant Velocity Based Staggered Implicit Finite Volume Scheme for Solving the Compressible/Incompressible Navier-Stokes Equations,'' The Third International Symposium on Experimental and Computational Aerothermodynamics of Internal Flows, Inst. of Engineering Thermophysics, Chinese Academy of Sciences, Beijing, PRC, Sept. 1996.

[20]Koren, B., ''Upwind Schemes, Multigrid and Defect Correction for the Steady Navier-Stokes Equations,'' *Proceedings of the 11th International Conference on the Numerical Methods in Fluid Dynamics*, edited by D. L. Dwoyer, M. Y. Hussaini, and R. G. Voigt, Springer–Verlag, Berlin, 1989.

[21]Liu, C., Liu, Z., and McCormick, S., ''Multigrid Methods for Numerical Simulation of Laminar Diffusion Flames,'' AIAA Paper 93-0236, Jan. 1993.

[22]Liu, C., and Liu, Z., ''High Order Difference and Multigrid Methods for Spatially-Evolving Instability in a Planar Channel,'' *Journal of Computational Physics*, Vol. 106, No. 1, 1993, pp. 92–100.

[23]Mitchell, R. E., ''Nitrogen Oxide Formation in Laminar Methane-Air Diffusion Flames,'' Sc.D. Dissertation, Massachusetts Inst. of Technology, Cambridge, MA, 1975.

[24]Mitchell, R. E., Sarofm, A. F., and Clomburg, L. A., ''Experimental and Numerical Investigation of Confined Laminar Diffusion Flames,'' *Combustion and Flame*, Vol. 37, 1980, pp. 227–244.

[25]Switzer, G., and Sturgess, G., ''Relation of CARS Temperature Fields to Lean Blowout Performance in an Aircraft Gas Turbine Generic Combustor,'' AIAA Paper 94-3271, June 1994.